crystals

MDPI

Article

Microstructure and Mechanical Properties of Laser Welded Magnesium Alloy/Steel Joint Using Cu-Si Composite Interlayer

Kai Yu, Min Lei *, Aori Zeng and Hua Zhang

Key Lab for Robot & Welding Automation of Jiangxi Province, School of Advanced Manufacturing, Nanchang University, Nanchang 330031, China; yukai@email.ncu.edu.cn (K.Y.); zarncu@163.com (A.Z.); hzhang@ncu.edu.cn (H.Z.)

* Correspondence: leimin@ncu.edu.cn

Abstract: In this study, Cu-Si composite powder was used as the interlayer to carry out laser lap deep penetration welding of AZ31B magnesium alloy and DP590 dual-phase steel. The effects of Cu-Si composite powder on the weld formation, microstructure, and mechanical properties of magnesium alloy and steel joint were studied. The results show that the addition of Si can improve the laser absorption rate of the interlayer and increase the melting depth at the magnesium side. In addition, the Cu-Si composite interlayer hindered the diffusion of Al, and reduced the thickness of reactive layer at the magnesium alloy and the steel interface. After adding Si into the interlayer, the reactive layer changed from Fe_3Al+α-Mg to Fe-(Al, Si) +α-Mg and the content of intermetallic compounds in the reactive layer decreased, which improved the plastic deformation capacity and the ductility of the reactive layer. As a result, the tensile shear force firstly increased and then decreased with the Si increase. The maximum tensile shear force of 86.2 N/mm was achieved when the Si content was 5%, which was 20.4% higher than that of the Cu interlayer. Plus, the fracture location changed from near the steel side to near the magnesium side weld.

Keywords: magnesium alloy; DP590 dual-phase steel; laser deep penetration welding; microstructure; mechanical properties

Citation: Yu, K.; Lei, M.; Zeng, A.; Zhang, H. Microstructure and Mechanical Properties of Laser Welded Magnesium Alloy/Steel Joint Using Cu-Si Composite Interlayer. *Crystals* **2022**, *12*, 1083. https://doi.org/10.3390/cryst12081083

Academic Editor: Pavel Lukáč

Received: 29 June 2022
Accepted: 29 July 2022
Published: 2 August 2022

1. Introduction

Lightweight is one of the important approaches to energy saving and emission reduction in the automotive industry. Furthermore, it is well known that the usage of lightweight metal is a good way to reduce the weight of automobile [1–3]. Magnesium alloy, as one of the lightest metal materials, possesses low density, high specific stiffness and strength, and good vibration absorption and noise reduction performance, which is widely used in automobile industry [4–6]. Steel is one of the leading materials widely used in various parts of automobile. Composite structure of magnesium alloy/steel has the advantages of reducing the overall weight and strengthening the local load-bearing, so joining of magnesium alloy and steel has also become one of the research hotspots. Compared with traditional welding methods, laser deep penetration welding has the advantages of high energy density, fast welding speed, low welding deformation, wide range of weldable materials, and high efficiency [7]. So, it has been widely used in joining dissimilar materials in recent years [8,9].

There are great differences in thermal physical properties such as thermal expansion coefficient and melting point between Mg and Fe. Moreover, neither solid solution nor intermetallic compound (IMC) exists in Mg/Fe system, according to the Mg-Fe phase diagram [10]. So, there are quite a lot of difficulties in obtaining reliable joint of magnesium alloy/steel [11]. Some researchers proposed that addition of appropriate interlayer in magnesium alloy/steel system modified the interfacial reaction and improved the mechanical properties. Song G [12,13] joined AZ31B magnesium alloy and Q235 low carbon steel by

hybrid laser-TIG double-side welding technique with Ni foil as an interlayer. The results showed that as the laser moved to the Fe side, more Fe melted, which increased the dissolution of Ni in Fe and the formation of (Fe, Ni) solid solution, finally inhibiting the reaction between Ni and Mg and reducing the formation of Mg_2Ni. It was beneficial to improve the tensile strength of the joint, and the maximum tensile strength reached 256 MPa. Tan CW [14] laser-welded AZ31B magnesium alloy and Ni-coating Q235 low carbon steel. The results showed that Ni could promote the metallurgical reaction of the joint. At lower laser power (1600 W), FeAl phase was generated in the laser irradiation area, AlNi phase was generated in the middle area, and AlNi phase and (α-Mg + Mg_2Ni) were generated in the weld toe zone. When the laser power increased to more than 2000 W, the FeAl phase became thicker, and a new Fe-Ni transition layer was formed in the middle zone and the weld toe zone. Liu LM [15–17] joined AZ31B magnesium alloy and Q235 low carbon steel by a hybrid laser-TIG welding technique using Cu and Ni as interlayer, respectively. It was found that with Cu as the interlayer, Mg_2Cu IMC was generated in the magnesium side weld; while with Ni as the interlayer, Mg_2Ni IMC was generated in the magnesium side weld. The result showed that the tensile strength of the joint with Cu as the interlayer (170 MPa) was higher than that with Ni (164 MPa). Liu proposed that the strengthening effect of Mg_2Cu distributing in a reticulate structure was better than that of Mg_2Ni with dispersive distribution, so the Cu interlayer was better than that of Ni. Ding M [18] joined ferritic stainless steel and magnesium alloy with Cu foil using the TIG-MIG hybrid method. Continuous and stable Al_3CuFe_4 IMC and Mg_2Cu IMC were generated at the magnesium alloy/steel interface, which improved the mechanical properties of joint. Plus, the maximum tensile strength of joint was 84 Mpa. In our previous study [19], AZ31B magnesium alloy and galvanized steel DP590 were laser welded with Cu interlayer. It was found that the addition of Cu promoted the uniform formation of Fe-Al IMCs and suppressed the generation of MgZn IMC at the Mg/Fe interface, which prohibited the formation of micro-fissure in Mg weld. What is more, the similar conclusion of Mg-Zn is consistent with the result of Cao R [20]. Moreover, the mechanical properties of the magnesium alloy and steel joint increased by 17% after addition of Cu interlayer. Additionally, some researchers found that Si could improve the mechanical properties of Fe-Al reactive layer, which finally increased the ductility and tensile strength of the joint. Hu YY [21] joined DP590 dual-phase steel and 6061 aluminum alloy by laser welding-brazing using Al-based welding wire with different Si content. It was found that because of the Si addition, Fe-Al phase transformed into Fe-(Al, Si) phase which had better ductility; moreover, the thickness of reactive layer was decreased. The result showed that the tensile strength of the joint increased by 72%. Xia HB [22] joined DP590 dual-phase steel and 6061-T6 aluminum alloy by laser welding-brazing with pure Al, AlSi5, and AlSi12 filler metals. It was found that the addition of Si effectively reduced the thickness of Fe_2Al_5 and $FeAl_3$ layer. Plus, the tensile strength of the joint with the AlSi5 filler metal increased by 43% compared to pure Al and increased by 11% compared to AlSi12. Therefore, the appropriate amount of Si could reduce the thickness of Fe-Al reaction layer and improve the ductility of the reaction layer. Based on both the advantages of Si and Cu, we considered adding Si into the Cu interlayer to further improve the mechanical properties of the joint. Till now there are a few research projects on the influence of the Cu-Si composite layer on microstructure and properties of magnesium alloy/steel welded joints.

In this study, Cu-Si composite powder was used as interlayer to laser-weld DP590 dual-phase steel and AZ31B magnesium alloy. The effect of the Cu-Si interlay on microstructure evolution and mechanical properties of the AZ31B magnesium alloy and DP590 dual-phase steel joint was investigated. The purposes of this research are to achieve magnesium/steel dissimilar jointing, enrich the joining theory of magnesium alloy and steel, and further promote the feasibility of magnesium alloy in the application of the automobile industry.

2. Materials and Methods

The base metals used in this study were AZ31B magnesium alloy and galvanized steel DP590. The chemical composition of the base materials is presented in Table 1. The interlayer was made of micron Cu and Si powder of 99.9% purity, and the thickness of the interlayer was 130 μm. Since the thickness of the powder on the surface of the base material was difficult to measure directly, the mass of the powder added in each experiment was 0.4 g, and the powder was spread evenly on the lap surface with an area of 20 mm × 45 mm.

Table 1. Composition of welding base material (wt. %).

Material	Al	Zn	Mn	Si	C	S	P	Fe	Mg
DP590	0.02	-	1.60	0.0466	0.068	0.015	0.011	Bal	-
AZ31B	3.12	0.95	0.15	0.10	-	-	-	0.03	Bal

A continuous fiber laser system (IPG YLS-2000TR) with a wavelength of 1060–1080 nm and the BPP of 8 mm·mrad was used. The laser beam has a diameter of 300 μm in the focal plane and the zero-defocus amount condition was when the lowest surface of the laser head was 47.00 mm from the top surface of the galvanized steel DP590 plate. Before welding, the base material was polished with #400 sandpaper to remove surface oxide film, then cleaned with alcohol to remove dust and oil, and then blown dry. In our previous study [19], the welding parameters of the Cu on welding quality had been determined. And, in this paper, we explored the influence of Cu-Si on microstructure and properties of magnesium alloy/steel welded joints. So, the same set of experimental parameters were used. During the welding experiment, the laser power was 800 W, the power density was 1131.77 kW/cm^2, the welding speed was 0.05 m/s, the defocus amount was 0 mm, and the shield gas (99.9% pure Ar) flux was 22 L/min. The lap configuration adopted in this study is shown in Figure 1. Each sample was repeated three times.

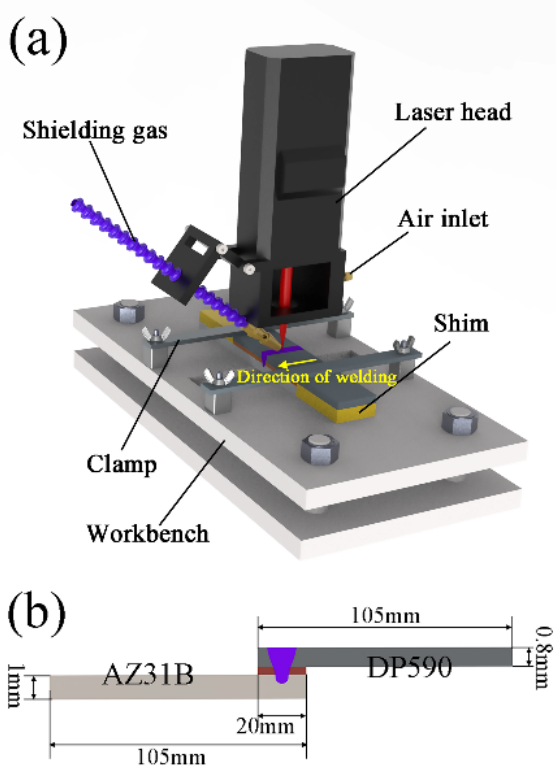

Figure 1. Schematic diagram of laser welding: (**a**) overall schematic diagram and (**b**) schematic diagram of lap joint.

After the welding experiment, the samples were cut by wire cutting perpendicular to the weld line for microstructure observation. Microstructure of the magnesium alloy and steel interfaces was observed by S-3200-NHITACHI scanning electron microscopy (SEM) with energy disperse spectroscopy (EDS). The interface phase characterizations were carried out using Rigaku SmartLab SE type micro-x-ray diffraction (micro-XRD) analysis. The hardness test was performed on both the steel side and magnesium alloy side by an HV-1000A microhardness tester with an applied load of 50 g and a holding time of 15 s. The microhardness and elastic modulus of the reactive layer was measured by Fischerscope HM2000 nano-indenter with a load of 150 mN, an indentation depth of 1 μm, and a holding time of 15 s. The specimen sample was cut along the vertical direction of the weld using wire cutting technology. Schematic diagram of tensile specimen size is shown in Figure 2. The tensile test of the joint was performed by a GTM2500 test machine, and the tensile rate was 1 mm/min at room temperature. The fracture characteristics and fracture morphology of the magnesium alloy-steel interface were analyzed by SEM.

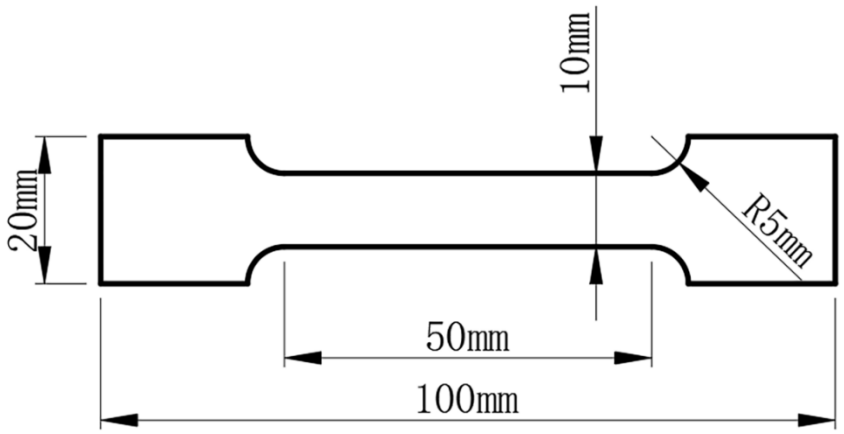

Figure 2. Schematic diagram of tensile specimen size.

3. Results and Discussion

3.1. Analysis of Surface Morphology and Microstructure

The weld surface morphology of magnesium alloy/steel joint is shown in Figure 3. It can be seen that the surface of the joint is well formed and the weld is continuous and uniform, and there are no obvious defects such as spatter and visible cracks on the surface of the base material. The backside of the weld is shown on the right side of Figure 3. It can be observed that the magnesium alloy at the bottom is not fully melted except at the starting and ending points of the weld. The weld appearance at the magnesium alloy side is shown in Figure 4. The magnesium alloy/steel interface all showed an arc shape from the middle to the steel side and some Fe blocks are observed in the weld at the magnesium alloy side. No visible welding defects such as cracks or air holes could be observed inside the weld. The melting depth and the melting width at the magnesium side are presented in Figure 5. It is shown that the melting depth increases with the increase of Si content and the melting width first increases and then decreases with the increase of Si content.

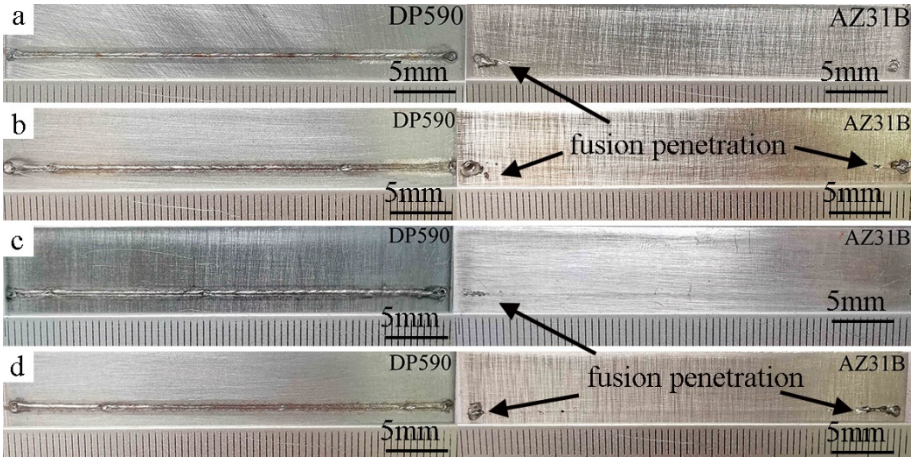

Figure 3. Weld surface morphology of joint: (**a**) Cu−0%Si, (**b**) Cu−2%Si, (**c**) Cu−5%Si, and (**d**) Cu−8%Si.

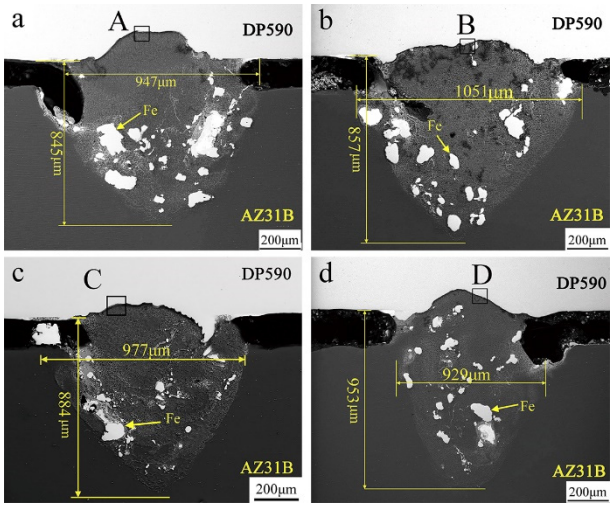

Figure 4. Weld appearance at the magnesium alloy side: (**a**) Cu−0%Si, (**b**) Cu−2%Si, (**c**) Cu−5%Si, and (**d**) Cu−8%Si.

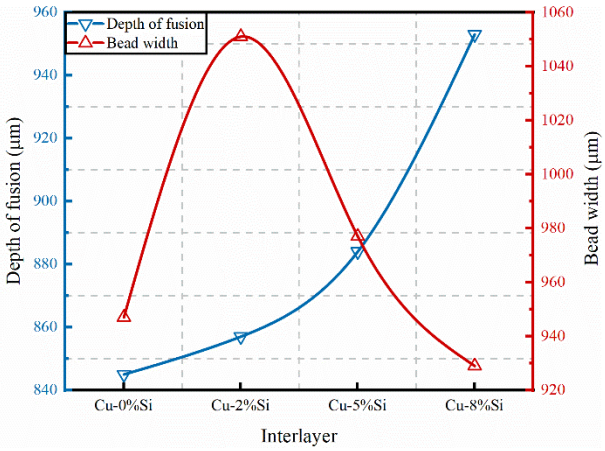

Figure 5. Curves of the melting depth and melting width with different Si content.

In our previous analysis [19], using Cu as an interlayer could enhance the efficiency of heat transfer between the magnesium alloy and steel, which can transfer more heat to the

magnesium alloy. In addition, the absorptivity of the material to the laser is related to the laser wavelength and the resistivity of the material itself, the relationship is shown as below [23]:

$$\alpha = 0.365\sqrt{\frac{\rho}{\lambda}} \quad (1)$$

where α is the absorptivity of the material to the laser beam; ρ is the resistivity of the material, in Ω·m; λ is the laser wavelength, and the unit is nm.

During the welding process, the wavelength of the laser remains constant. It can be seen from the above formula that when the laser wavelength maintains at a certain level, the laser absorptivity of the material depends on the resistivity of the material. The higher the resistivity is, the higher the laser absorptivity of the material is. The resistivity of Si is 2.52×10^{-4} (Ω·m), which is significantly higher than that of Cu (1.7×10^{-8} (Ω·m)) [24]. Therefore, the resistivity of Cu-Si composite powder is higher than that of pure Cu powder. With the increase of Si content, the resistivity of the composite powder also increases, which enhances the absorptivity of laser by the interlayer. So, the absorption of laser by magnesium alloy also increases accordingly, which increases the melting depth of the magnesium alloy side. In addition, the element Si can increase the specific heat of the liquid metal in the molten pool. According to the theory of Li CL [25], the increase of specific heat of liquid metal can increase the laser power absorbing in the molten pool during the laser welding process, which can finally increase the melting depth at the magnesium alloy side.

3.2. Microstructure Distribution at Magnesium Alloy-Steel Interface

From Figure 4, it can be seen that light-colored phase distributes in blocks or particles inside the weld at the magnesium alloy side; and the light-colored phase is significantly reduced after the addition of Si. The EDS analysis shows that the light-colored phase is mainly composed of Fe (80.39 at. %), which indicates that the addition of Si can effectively inhibit the un-melted Fe from reaching molten pool at the magnesium side.

In order to investigate the effects of Cu and Si on the microstructure of the Mg-Fe interface of the joint, the middle part of the Mg-Fe interface in Figure 4 (marked as A, B, C, and D) in Figure 4 was selected for magnified observation. Furthermore, the magnification interface is shown in Figure 6; the EDS point analysis at each point in Figure 6 is shown in Table 2. It can be seen from Figure 6 that there is an obvious gray reactive layer at the magnesium alloy and steel interface, and the thickness of the reactive layer decreases with the increase of Si content in the interlayer. In addition, obvious air holes are observed in the weld at the magnesium alloy side when the Si content in the interlayer is 0%, 2%, and 5%, as shown in Figure 6a, Figure 6b, and Figure 6d, respectively. Moreover, a small number of cracks are also observed in the weld when the Si content is 2%, as shown in Figure 6b. However, when the Si content is 5% no obvious welding defects are observed (Figure 6c).

In order to further analyze the composition of different IMCs, EDS test was conducted at different points, and the result is shown in Table 2. It shows that reactive layer is composed of Fe, Mg, and Al when the Si is 0% (Point 1). Plus, the content of Al in the reactive layer reaches 14.00 %, which comes from the magnesium alloy base metal. Combined with the Fe-Al binary phase diagram [26], the phase at Point 1 is deduced to be Fe_3Al+α-Mg. The Si content in the reactive layer reaches 5.48% when the interlayer is Cu-5%Si (Point 4), so the reactive layer is deduced to be Fe-(Al, Si) +α-Mg, in which Si substitutes Al elements or fills the lattice vacancies [27]. The weld at the magnesium side is consisted of the dark matrix and the light reticular phase. The dark matrix (Point 2 and Point 5) is mainly composed of Mg, which should be α-Mg, and the white reticular phase (Point 3 and Point 6) is mainly composed of Mg and Cu, and a small amount of Al. Combined with the Al-Mg-Cu ternary phase diagram [28], it should be the $(Mg, Al)_2Cu$ phase, which was also observed in the arc spot welding of AZ31 Mg alloy to Q235 steel with Cu as interlayer system according to [29].

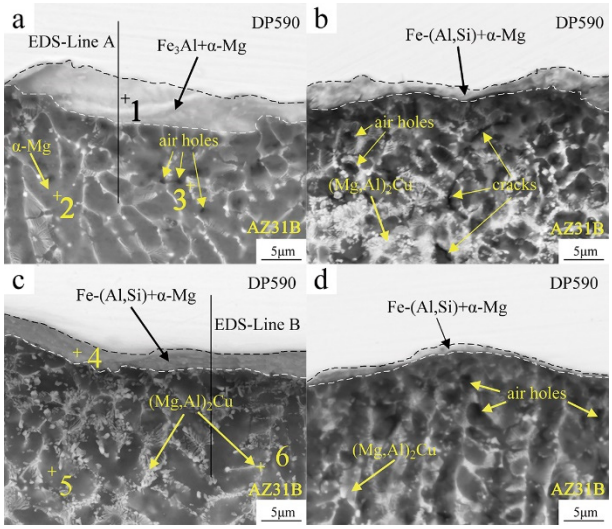

Figure 6. Magnification of magnesium alloy-steel interface: (**a**) magnification of Zone A (Cu−0%Si), (**b**) magnification of Zone B (Cu−2%Si), (**c**) magnification of Zone C (Cu−5%Si), and (**d**) magnification of Zone D (Cu−8%Si).

Table 2. The results of EDS analysis at each point in Figure 6 (at. %).

Point	Fe	Mg	Al	Cu	Zn	Si	Possible Phase
1	50.89	31.78	14.00	2.37	0.97	–	Fe_3Al+α-Mg
2	0.59	92.47	1.63	1.93	3.38	–	α-Mg
3	–	70.47	4.13	23.14	–	–	$(Mg, Al)_2Cu$
4	22.44	53.24	12.04	5.08	1.62	5.48	Fe-(Al, Si) +α-Mg
5	1.01	92.56	1.89	3.22	1.14	0.19	α-Mg
6	1.43	69.42	4.4	18.75	5.17	0.83	$(Mg, Al)_2Cu$

In order to further determine the phase of the reactive layer, micro-XRD analysis was performed on the reactive layer of the magnesium alloy/steel joint. The results are shown in Figure 7. It shows that the intermetallic compounds of Cu−0%Si and Cu−5%Si reactive layer are Fe_3Al+α-Mg and Fe-(Al, Si) +α-Mg, respectively, which are consistent with the EDS results of Table 2.

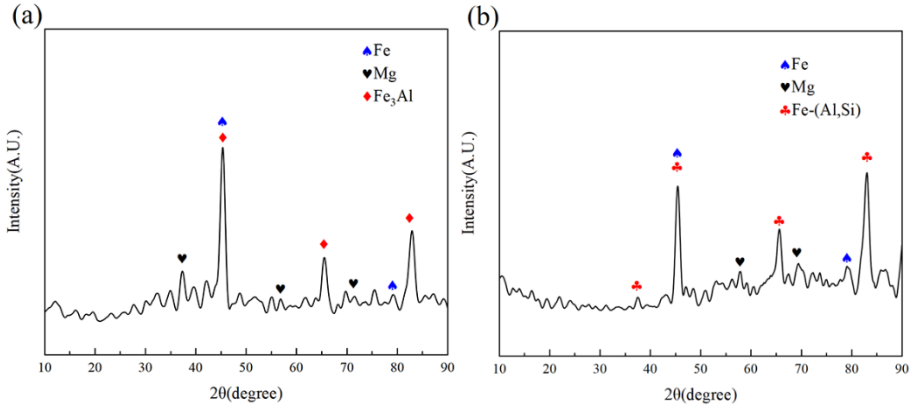

Figure 7. micro-XRD patterns of the reactive layer with different Si contents: (**a**) Cu−0%Si and (**b**) Cu−5%Si.

Results of the EDS line and map analysis at the middle of the magnesium alloy/steel interface for Cu−0%Si and Cu−5%Si are shown in Figures 8 and 9, respectively. It can be seen that both the Al and Fe content increase significantly and the content of Mg fluctuate

obviously at the Mg/Fe interface, which verifies the existence of both the Fe-Al phase and the α-Mg phase. The EDS line analysis and map analysis show a low Si content in the whole reactive layer; moreover, the content of Mg in the reactive layer is much higher than that without Si addition in the interlayer. Combined with the micro-XRD analysis, it indicates that the addition of Si transforms Fe_3Al IMC into Fe-(Al, Si) IMC, and the content of IMC in the reactive layer decreases. It can be measured that the thickness of the reactive layer is 6.7 μm and 4.0 μm when the interlayer is Cu−0%Si and Cu−5%Si, respectively, as shown in Figure 8. According to Pouranvari, M [30], Si can inhibit the diffusion of Al to the Fe side, so the thickness of the reactive layer decreases with Si addition in the interlayer.

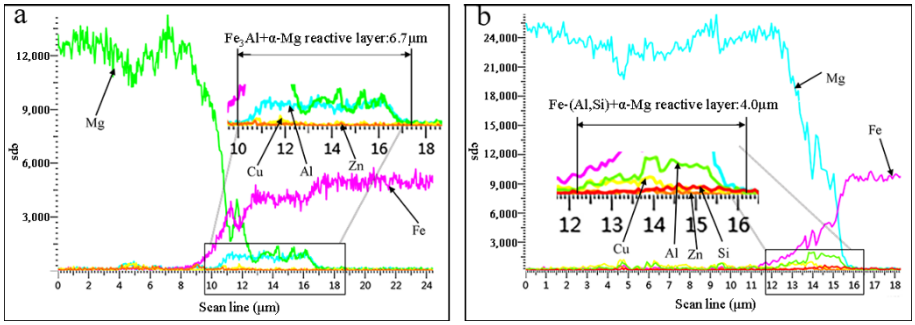

Figure 8. EDS line scanning of line A and line B of magnesium alloy/steel interface in Figure 6: (**a**) line A (Cu−0%Si) and (**b**) line B (Cu−5%Si).

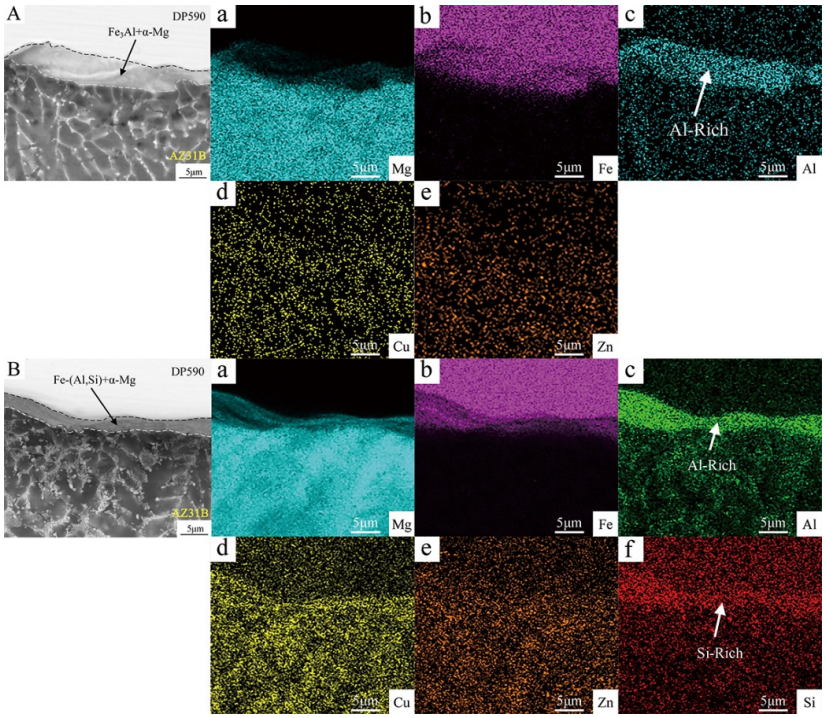

Figure 9. EDS map analysis at the magnesium alloy/steel interface in Figure 6: (**A**) Cu−0%Si and (**B**) Cu−5%Si.

3.3. Mechanical Analysis

The microhardness test was carried out through the weld at both the steel side and the magnesium alloy side. Plus, the microhardness distribution of the magnesium alloy/steel joint with Cu−0%Si and Cu−5%Si interlayer is shown in Figure 10, respectively. It can be found that the microhardness of the joint presents a "convex" shape with the center of the weld as the axis of symmetry. The microhardness of the fusion zone (FZ) at both

the steel side and the magnesium alloy side is the biggest, followed by the heat-affected zone (HAZ), and the lowest in the base material (BM), which is consistent with the result of Tao T [31], who laser lap welded AZ31B-alloy to DP590-steel. The average hardness of the weld at the steel side with the Cu−5%Si interlayer (267.5 HV) is slightly higher than that with Cu−0%Si (263.1 HV). This is because Si can enhance the hardness of the steel [32]. During the welding process, a small amount of Si enters the steel side, which can enhance the hardness of the weld at the steel side.

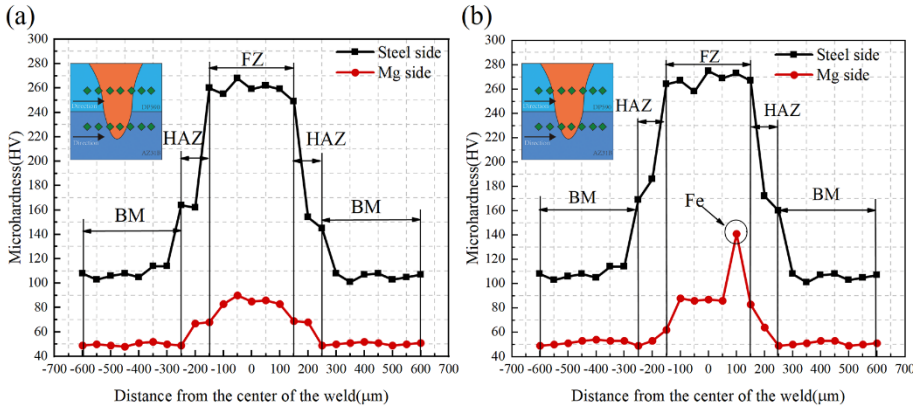

Figure 10. Microhardness of joints without Si and with 5%Si: (**a**) Cu−0%Si and (**b**) Cu−5%Si.

The hardness and elastic modulus of the reactive layer with Cu−0%Si and Cu−5%Si interlayer are shown in Figure 11a, respectively. Both the hardness and the elastic modulus of the reactive layer with the Cu−5%Si interlayer is much lower than those with the Cu−0%Si, as shown in Figure 11a. The load–displacement curves of different reactive layers are shown in Figure 11b. The results indicate that the plastic deformation capacity of the reactive layer improves and the ductility of the reactive layer increases when the reactive layer transforms from Fe_3Al+α-Mg to Fe-(Al, Si) +α-Mg. This is beneficial for the release of residual stress in the joint and could improve the mechanical properties of the joints.

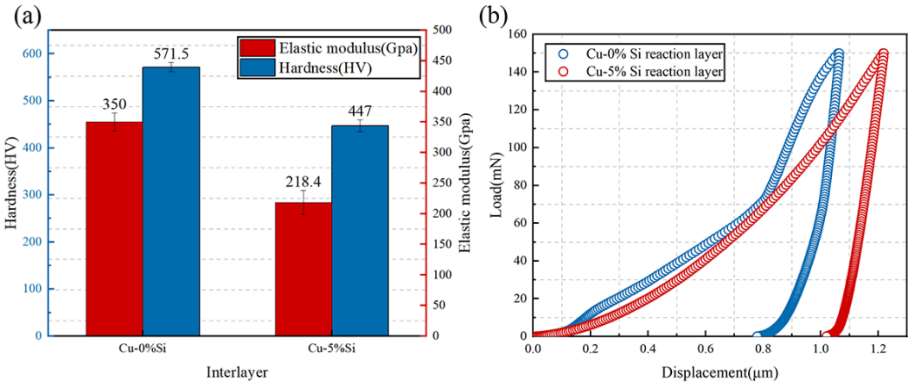

Figure 11. Hardness and elastic modulus of the reaction layer and load–displacement curves: (**a**) hardness and elastic modulus of reaction phase and (**b**) load–displacement curves.

In this paper, the tensile shear force of magnesium alloy/steel lap joint was characterized by the load per unit length of weld. The relationship is shown as below:

$$F = \frac{F_{max}}{l} \quad (2)$$

where F_{max} is the maximum load of joint fracture, and the unit is N; l is the length of weld, and the unit is mm.

The tensile shear force of the magnesium alloy/steel joint with different Si content in the interlayer is shown in Figure 12. The tensile shear force firstly increases and then

decreases with the increase of Si in the Cu interlayer. When Si content is 5%, the tensile shear force of the joint reaches the maximum of 86.2 N/mm, which is about 20.4% higher than with pure Cu interlayer. From the analysis of microstructure and nano-indentation, it is found that the addition of Si transforms Fe_3Al IMC into Fe-(Al, Si) IMC and decreases the content of IMC in the reactive layer, which improves the ductility of the reactive layer. Furthermore, the thickness of the reactive layer is greatly decreased, which is also beneficial for the improvement of mechanical properties. However, with the further increase of Si content, the weld at the magnesium alloy side generates a large number of cracks, which reduces the tensile shear force of the joint.

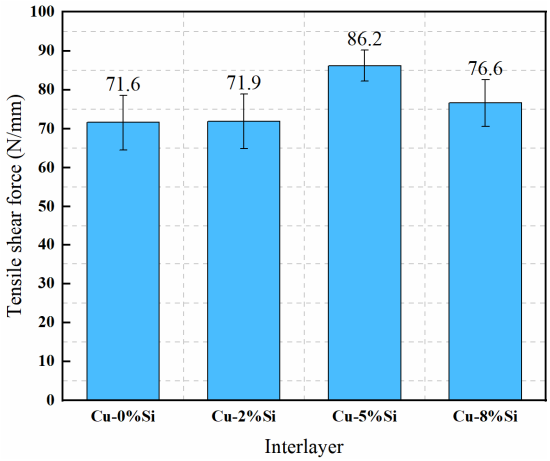

Figure 12. Tensile shear force of the magnesium alloy/steel joint.

The macroscopic morphology of the fracture of the Cu−0%Si and Cu−5%Si joint and the cross-sectional after the tensile test are shown in Figure 13, respectively. It can be seen from Figure 13a,b that quite a lot of unmelted Cu remains at the magnesium alloy side near the fracture surface with the Cu-0%Si interlayer, which is not observed near the fracture surface with the Cu−5%Si interlayer. Moreover, the spatter on the magnesium alloy with Cu−0%Si interlayer is more than Cu−5%Si layer. From the cross section of the fracture shown in Figure 13c,d, it can be observed that the joint without and with Si addition fractures on the weld near the steel side and near the magnesium alloy side, respectively. In addition, the fracture location of the joint with Si addition presents a more tortuous cracking shape and much more secondary cracks, which indicates that it absorbs more energy during the tensile shear test.

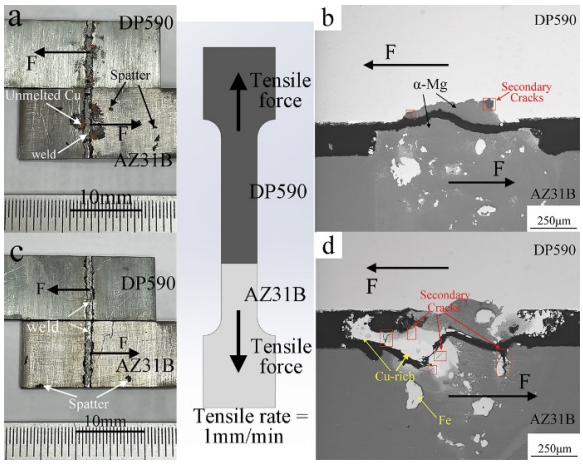

Figure 13. Macroscopic appearance of fracture and cross section display after tensile shearing: (**a**) Cu−0%Si, (**b**) Cu−0%Si cross section display, (**c**) Cu−5%Si, and (**d**) Cu−5%Si cross section display.

4. Conclusions

Laser lap deep penetration welding of AZ31B magnesium alloy and DP590 dual-phase steel with Cu-Si composite interlayer was carried out in this study. The effects of the addition Si on interfacial microstructure and mechanical properties were studied. The main conclusions are as follows:

(1) A well-formed and no obvious defects weld can be obtained with both Cu and Cu-Si interlayer. The addition of Si improves the laser absorption rate of the interlayer, which increases the melting depth at the magnesium side.

(2) The microstructure at the interface with Cu interlayer consists mainly of Fe_3Al phase and α-Mg phase. After adding Si into the interlayer, Fe_3Al IMC converts to Fe-(Al, Si) IMC, and the content of IMC in the interlayer decreases. Moreover, the thickness of the reactive layer reduces gradually with the increase of Si content.

(3) The addition of Si improves the plastic deformation capacity and the ductility of the reactive layer. The hardness and elastic modulus of the reactive layer reduced from 571.5 HV and 350 Gpa (Cu−0%Si) to 447 HV and 218.4 Gpa (Cu−5%Si), respectively. The tensile shear force firstly increases and then decreases with the Si increase. The maximum tensile shear force of 86.2 N/mm is achieved when the Si content is 5%, which is 20.4% higher than that of the Cu interlayer. The fracture location changes from near the steel side (Cu−0%Si) to near the magnesium side weld (Cu−5%Si).

Author Contributions: Funding acquisition, M.L. and H.Z.; investigation, K.Y. and A.Z.; methodology, A.Z. and K.Y.; writing–original draft, K.Y.; formal analysis, K.Y.; writing—review & editing, M.L. All authors have read and agreed to the published version of the manuscript.

Funding: This research was funded by [Jiangxi Provincial Superior Science and Technology Innovation Team Project] grant number [20181BCB24001], [Natural Science Foundation of Jiangxi] grant number [20202BAB214020] and [National Natural Science Foundation of China] grant number [52105354].

Data Availability Statement: Not applicable.

Conflicts of Interest: The authors declare no conflict of interest.

References

1. Wang, J.; Zhou, L.; Jiang, X.; Hu, S. Influence of forming parameters on temperature and surface quality for AZ31B magnesium alloy sheet during incremental forming. *Forg. Stamp. Technol.* **2020**, *45*, 47–54.
2. Li, G.; Liu, X. Literature review on research and development of automotive lightweight technology. *Mater. Sci. Technol.* **2020**, *28*, 47–61.
3. Kaluza, A.; Kleemann, S.; Frohlich, T.; Herrmann, C.; Vietor, T. Concurrent design & life cycle engineering in automotive lightweight component development. In Proceedings of the 1st CIRP Conference on Composite Materials Parts Manufacturing (CIRP CCMPM), Karlsruhe Institute of Technology, Karlsruhe, Germany, 8–9 June 2017; pp. 16–21.
4. Friedrich, H.; Schumann, S. Research for a "new age of magnesium" in the automotive industry. *J. Mater. Process. Technol.* **2001**, *117*, 276–281. [CrossRef]
5. Wahba, M.; Katayama, S. Laser welding of AZ31B magnesium alloy to Zn-coated steel. *Mater. Des.* **2012**, *35*, 701–706. [CrossRef]
6. Subravel, V.; Alagappan, N.; Babu, N. Influence of arc oscillation frequency on tensile properties and microstructural characteristics of magnetic arc oscillation welded AZ31B magnesium alloy joints. *Mater. Today-Proc.* **2020**, *22*, 606–613. [CrossRef]
7. Wang, Z.; Jiang, S.; Chen, Y.; Xiong, Z.; Hu, D.; Cheng, D. Numerical simulation of laser welding of magnesium and steel dissimilar metal based on ABAQUS. *Trans. Mater. Heat Treat.* **2021**, *42*, 134–141.
8. Yang, F.; Xia, G.J.; Guo, X.; Chen, C.Y.; Long, Y.; Chen, B.H.; Tang, J.L.; Chen, G.Y. Research progress of laser welding under subatmospheric pressure. *Int. J. Adv. Manuf. Technol.* **2021**, *116*, 803–820. [CrossRef]
9. Cao, X.; Jahazi, M.; Immarigeon, J.P.; Wallace, W. A review of laser welding techniques for magnesium alloys. *J. Mater. Process. Technol.* **2006**, *171*, 188–204. [CrossRef]
10. Nayeb-Hashemi, A.A.; Clark, J.B.; Swartzendruber, L.J. The Fe−Mg (Iron-Magnesium) system. *Bull. Alloy Phase Diagr.* **1985**, *6*, 235–238. [CrossRef]
11. Song, G.; Li, T.T.; Yu, J.W.; Liu, L.M. A Review of Bonding Immiscible Mg/Steel Dissimilar Metals. *Materials* **2018**, *11*, 2515. [CrossRef]
12. Song, G.; Li, T.T.; Chi, J.Y.; Liu, L.M. Bonding of immiscible Mg/steel by butt fusion welding. *Scr. Mater.* **2018**, *157*, 10–14. [CrossRef]

13. Song, G.; Li, T.T.; Zhang, Z.D.; Liu, L.M. Investigation of unequal thickness Mg/steel butt-welded plate by hybrid laser-tungsten inert gas welding with a Ni interlayer. *J. Manuf. Process.* **2017**, *30*, 299–302. [CrossRef]
14. Tan, C.W.; Xiao, L.Y.; Liu, F.Y.; Chen, B.; Song, X.G.; Li, L.Q.; Feng, J.C. Influence of Laser Power on the Microstructure and Mechanical Properties of a Laser Welded-Brazed Mg Alloy/Ni-Coated Steel Dissimilar Joint. *J. Mater. Eng. Perform.* **2017**, *26*, 2983–2997. [CrossRef]
15. Liu, L.M.; Qi, X.D. Strengthening effect of nickel and copper interlayers on hybrid laser-TIG welded joints between magnesium alloy and mild steel. *Mater. Des.* **2010**, *31*, 3960–3963. [CrossRef]
16. Liu, L.M.; Qi, X.D. Effects of copper addition on microstructure and strength of the hybrid laser-TIG welded joints between magnesium alloy and mild steel. *J. Mater. Sci.* **2009**, *44*, 5725–5731. [CrossRef]
17. Liu, L.; Qi, X.; Zhang, Z. The Effect of Alloying Elements on the Shear Strength of the Lap Joint of AZ31B Magnesium Alloy to Q235 Steel by Hybrid Laser-TIG Welding Technique. *Metall. Mater. Trans. A* **2012**, *43*, 1976–1988. [CrossRef]
18. Ding, M.; Liu, S.S.; Zheng, Y.; Wang, Y.C.; Li, H.; Xing, W.Q.; Yu, X.Y.; Dong, P. TIG-MIG hybrid welding of ferritic stainless steels and magnesium alloys with Cu interlayer of different thickness. *Mater. Des.* **2015**, *88*, 375–383. [CrossRef]
19. Zhang, H.; Zeng, A.; Xu, L.; Yang, F.; Zou, P.; Lei, M. Characteristics of Laser Deep Penetration Welding of Mg Alloy/Steel Controlled by Cu. *Chin. J. Rare Met.* **2021**, *45*, 804–811.
20. Cao, R.; Chang, J.H.; Huang, Q.; Zhang, X.B.; Yan, Y.J.; Chen, J.H. Behaviors and effects of Zn coating on welding-brazing process of Al-Steel and Mg-steel dissimilar metals. *J. Manuf. Process.* **2018**, *31*, 674–688. [CrossRef]
21. Hu, Y.Y.; Zhang, Y.M.; Mi, G.Y.; Wang, C.M.; Zhang, W.; Zhang, X. Effects of Si contents in filling wires on microstructure evolution and properties of Al-steel dissimilar joint by laser welding-brazing. *J. Mater. Res. Technol.* **2021**, *15*, 1896–1904. [CrossRef]
22. Xia, H.B.; Zhao, X.Y.; Tan, C.W.; Chen, B.; Song, X.G.; Li, L.Q. Effect of Si content on the interfacial reactions in laser welded-brazed Al/steel dissimilar butted joint. *J. Mater. Process. Technol.* **2018**, *258*, 9–21. [CrossRef]
23. Zhou, D.; Liu, J.; Lu, Y.; Zhou, L.; Pan, J. Microstructure and Mechanical Properties of Deep Penetration Laser Welding Joints in Steel/Aluminum with Si Powder Addition. *J. Mech. Eng.* **2018**, *54*, 58–65. [CrossRef]
24. Rathod, M.J.; Kutsuna, M. Joining of aluminum Alloy 5052 and low-carbon steel by laser roll welding. *Weld. J.* **2004**, *83*, 16S–26S.
25. Li, C.; Fan, D.; Yu, X.; Yu, S. Method of Arc-Assisted Laser Wire Welding-Brazing Between Aluminum and Galvanized Steel with Filler Powder. *Chin. J. Lasers* **2016**, *43*, 0702007.
26. Stein, F.; Palm, M. Re-determination of transition temperatures in the Fe-Al system by differential thermal analysis. *Int. J. Mater. Res.* **2007**, *98*, 580–588. [CrossRef]
27. Shi, Y.; Li, J.; Huang, J.; Gu, Y.; Fan, D. Effects of Si and Zn on interface microstructures of aluminum/steel welding-brazing joint. *Chin. J. Nonferrous Met.* **2015**, *25*, 30–35.
28. Richards, R.W.; Jones, R.D.; Clements, P.D.; Clarke, H. Metallurgy of Continuous Hot-Dip Aluminizing. *Int. Mater. Rev.* **1994**, *39*, 191–212. [CrossRef]
29. Ren, D.X.; Liu, L.M. Interface microstructure and mechanical properties of arc spot welding Mg-steel dissimilar joint with Cu interlayer. *Mater. Des.* **2014**, *59*, 369–376. [CrossRef]
30. Pouranvari, M.; Abbasi, M. Dissimilar gas tungsten arc weld-brazing of Al/steel using Al-Si filler metal: Microstructure and strengthening mechanisms. *J. Alloys Compd.* **2018**, *749*, 121–127. [CrossRef]
31. Tao, T.; Liu, J.; Zhou, D.; Li, H. Influence of laser-Sn powder coupling on microstructure and mechanical properties of fusion welded AZ31B-alloy to DP590-steel. *Opt. Laser Technol.* **2022**, *152*, 108091. [CrossRef]
32. Wang, G.; Wang, Q.; Che, H.; Li, Y.; Lei, M. Effects of Silicon on the Microstructure and Properties of Cast Duplex Stainless Steel with Ultra-HighChromium and High Carbon. *Acta Metall. Sin.* **2020**, *56*, 278–290. [CrossRef]